ACS APPLIED MATERIALS & INTERFACES

www.acsami.org
Research Article

Rapid and High-Density Antibody Immobilization Using Electropolymerization of Pyrrole for Highly Sensitive Immunoassay

USun Nam, Han Na Suh, Sang-Keun Sung, ChaeWon Seo, Jung Hyun Lee, Jeong Yoon Lee, SangHee Kim, and JuKyung Lee*

Cite This: ACS Appl. Mater. Interfaces 2024, 16, 30611−30621
Read Online

ACCESS | Metrics & More | Article Recommendations | Supporting Information

ABSTRACT: Polypyrrole (Ppy) is a biologically compatible polymer that is used as a matrix, in which drugs and enzymes can be incorporated by doping. Here, we suggest an inventive application of Ppy as a biorecognition film encapsulated with an antibody (Ab) as an alternative strategy for the on-site multistep functionalization of thiol-based self-assembled monolayers. The fabrication steps of the recognition films were followed by dropping pyrrole and Ab mixed solutions onto the electrode and obtaining a thin film by direct current electropolymerization. The efficiency of Ab immobilization was studied by using fluorescence microscopy and electrochemical (EC) methods. Finally, the Ab density was increased and immobilized in 1 min, and the sensing performance as an EC immunosensor was demonstrated using α-fetoprotein with a limit of detection of 3.13 pg/mL and sensing range from 1 pg/mL to 100 ng/mL. This study demonstrates the potential for electrochemical functionalization of biomolecules with high affinity and rapidity.

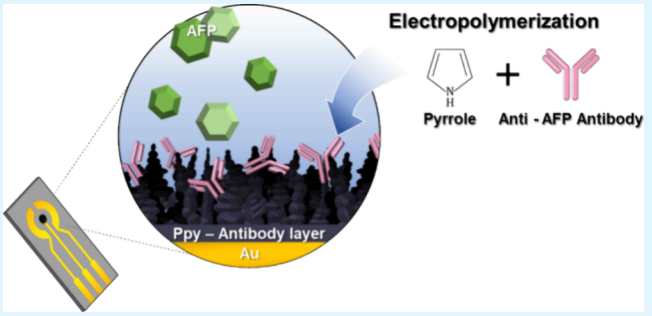

KEYWORDS: *conducting polymers, electropolymerization, biorecognition, polypyrrole (Ppy), α-fetoprotein (AFP)*

1. INTRODUCTION

Electrochemical (EC) immunosensors have been used to analyze a target analyte in a complex mixture such as body fluid and have been applied for disease diagnosis, environmental monitoring, and single-cell monitoring.[1−4] EC immunosensors have many advantages over various types of immunoassays, such as enzyme-linked immunosorbent assay (ELISA),[5] fluorescence immunoassay (FIA),[6] and surface plasmon resonance (SPR).[7] EC immunosensors are used for rapid and inexpensive analysis with a low limit of detection (LOD).[8−11]

The output module is easily integrated with wireless data collection/transmission systems and is easy to apply to wearable sensors.[12,13] The most important factor in EC immunosensors is the biorecognition layer, which interacts with the biological analyte. This biorecognition layer plays a role in target analyte specificity for biosensors such as antigen (Ag)−antibody (Ab) interactions.[14] Ab immobilization determines the immunological recognition and immunosensor performance.

The increase in the amount of Ab on the electrode surface is a solution to increase the sensitivity and specificity. Surface modification using self-assembled monolayers (SAMs) based on thiolated hydrocarbon molecules is a well-known covalent bond between the gold electrode surface and Ab.[15−18] Gold electrodes are used most frequently because gold is rigid and does not have a stable oxide layer. The first step in the formation of alkanethiol is the adsorption of the thiol group (−SH) onto the gold surface through the formation of the gold−thiol bond. The other terminal group has an amine ($-NH_2$) or carboxylic acid group (−COOH), which has the advantage that it makes covalent bonding to Abs. However, these SAMs were limited to thiol-modified gold substrates and did not consider the surface density of immobilized Ab.[19] Additionally, the formation of the SAMs takes a long time, from 1 h to 1 day.

In order to overcome the above-mentioned limitation, we designed an immobilization method for Abs to increase the Ab density based on the electropolymerization of pyrrole. Polypyrrole (Ppy) is a material of particular interest in EC sensors because of it has good biocompatibility and easy and simple immobilization of several biomolecules.[20−22] Various types of Ppy mixed layers are used for the selective detection of enzymes,[23,24] neurotransmitters,[25] and catechols.[26] Ppy is also used as a drug delivery material because it exhibits electro-

Received: January 14, 2024
Revised: May 21, 2024
Accepted: May 28, 2024
Published: June 10, 2024

chemically induced volume change due to the movement of ions and solvents in and out of the polymer matrix when a potential is applied.[27,28] In our previous work, we synthesized various types of Ppy morphologies using sodium perchlorate ($NaClO_4$) as a dopant. The cloud morphology was grown on the electrode surface, and the density and thickness of the Ppy films were investigated by applying the potential and applying time. During the formation of Ppy, the molecules and materials of the pyrrole solutions were also adsorbed on the electrode as a mixing compound of Ppy layers. Figure 1a illustrates the

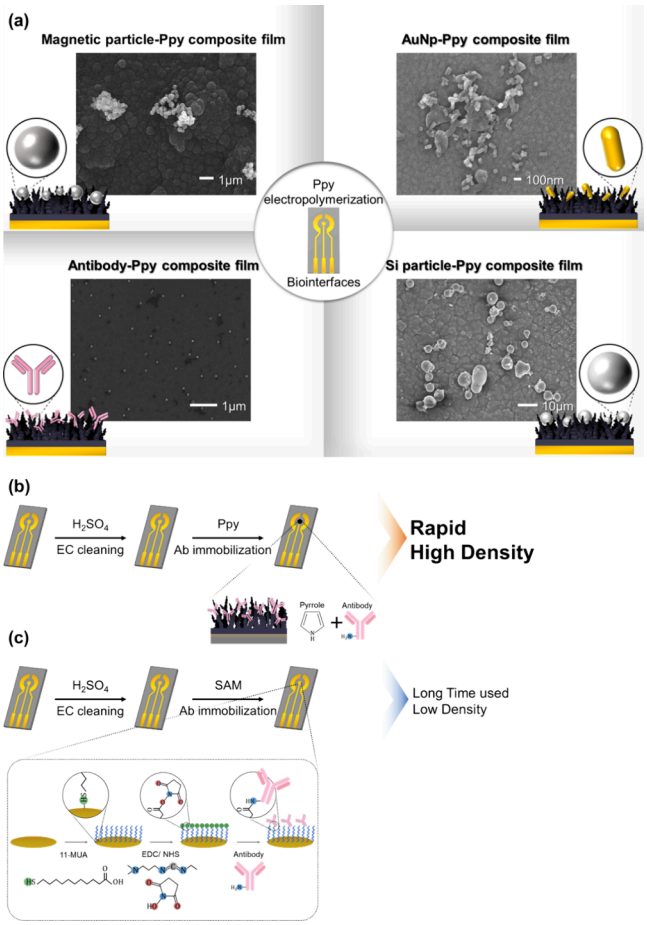

Figure 1. (a) Schematic illustration of various types of immobilization based on electropolymerization of pyrrole. (b) Schematic of immobilization of construction process of Ab based on the Ppy composite film. (c) Construction of the Ab recognition layer based on SAMs.

various types of Ppy mixing layers comprising gold nanoparticles, silicon particles, and magnetic nanoparticles. Similarly, mixing solutions of pyrrole and Ab electropolymerization was performed. As a result, Ab−Ppy layers were developed on the electrode surface in 1 min. This method is a one-step immobilization method, because additional treatment was not necessary to bind Ab. Thus, an Ab−Ppy mixing layer was developed, and we observed that the Ab density was increased compared with that of the SAMs-treated electrode. The feasibility of the immunosensor based on EC analysis was demonstrated by the quantification of α-fetoprotein (AFP) as a model analyte. AFPs are plasma proteins with low molecular weight (70 kDa) and are produced by the fetal liver during fetal development.[29−31] Elevated AFP levels lead to various diseases such as liver cancer, Down syndrome, and neural tube defects.[32,33] AFP is observed in the body and is an important biomarker for the diagnosis, recurrence, and prognosis of an illness. Finally, we observed that this Ppy immunosensor has an LOD of 3.13 pg/mL. Specificity using different analytes, stability, and reproducibility were also investigated.

Ab immobilization strategy using electropolymerization of pyrrole is a universal and direct assay to adsorb Ab on the electrode compared with multistep immobilization such as linker-mediated and layer-free immobilization using the F_c binding domain or protein A/G. In this multistep process, functionalized pyrrole (1*H*-pyrrole-1-propionic acid, pyrrole-2-carboxaldehyde)[34,35] was widely used. However, to the best of our knowledge, this study is the first attempt to direct an Ab mixing layer on an electrode using pyrrole without any functional group and the first attempt to apply this method to the immunosensing of a specific biomarker. The greatest advantage of this method is that it is easy and rapid (in 1 min) to construct an Ab layer, and Ab the high density of the Ab layer can be developed; some of the Ab has random orientation compared to the multistep immobilization method.

2. EXPERIMENTAL SECTION/METHODS

2.1. Reagents and Chemicals. Human anti-AFP Ab and AFP Ag were purchased from Abcam (Cambridge, MA, USA). Human anti-interleukin-6 (IL-6) Ab and IL-6 Ag were obtained, provided from R&D Systems (Minneapolis, MN, USA). Pyrrole monomer, $NaClO_4$, sulfuric acid (H_2SO_4), potassium chloride (KCl), 11-mercaptoundecanoic acid (11-MUA), *N*-(3-(dimethylamino)propyl)-*N*′-ethylcarbodiimide (EDC), *N*-hydroxysuccinimide (NHS), bovine serum albumin (BSA), potassium ferricyanide ($K_3Fe(CN)_6$), potassium ferrocyanide ($K_4Fe(CN)_6$), ethanolamine hydrochloride, goat anti-mouse immunoglobulin G (IgG) H&L (Alexa Fluor-488 labeled), fetal bovine serum (FBS), phosphate-buffered saline (10 mM PBS), 0.05% PBS between 20 (PBST), and all other analytical grade chemicals were purchased from Sigma−Aldrich (St. Louis, MO, USA).

2.2. Apparatus and Electrode. The commercial Au-screen-printed electrode (SPE; Model no. DRP C220AT, Φ = 4 mm; DRP C223AT, Φ = 1.6 mm), which consists of a working electrode (WE), counter electrode (CE), and reference electrode (RE), was purchased from Metrohm (Asturias, Spain). Cyclic voltammetry (CV), square-wave voltammetry (SWV), and EC impedance spectroscopy (EIS) were performed using a multichannel potentiostat obtained from Biologic Co (Paris, France; Model VMP3). All EC measurements were performed at room temperature (RT) in a Faraday cage to ensure electromagnetic shielding.

2.3. Fabrication of Electrode. The electrode was fabricated by using an e-beam evaporator (SNTek, Korea). An 8 in. Si wafer was cleaned with piranha solution (H_2SO_4:H_2O_2 = 4:1) and placed in an e-beam chamber with an aligned film mask (Microtech, Korea). A 200 nm Au layer was deposited by following a Ti adhesion layer (30 nm). A shielding layer was deposited using SU-8 photoresist (MicroChem, USA) to increase the sensitivity of the EC sensor. After UV cross-linking, the substrate was developed and rinsed using an SU-8 developer (MicroChem, USA).

2.4. Construction of Ab-Ppy SPE. The electrode was precleaned by using H_2SO_4. The SPE was immersed in a 10 mM H_2SO_4 solution with two CV scans, with a scan range from 0 to 1.8 V. This sequence was used to remove dust by EC cleaning. Ab was immobilized by the electropolymerization of pyrrole. A 1 μg/mL amount of anti- AFP Ab was mixed with 0.1 M monomer pyrrole/0.05 M $NaClO_4$ in PBS and prepared as an Ab−pyrrole mixing solution. The mixing solutions were dropped onto precleaned and precleaned SPE, and direct current electropolymerization (DCeP) was performed by simple chronoamperometry. The DC potential was fixed at 650 mV, and the potentials were applied for 1 min (Figure 1b). Finally, the modified electrode

https://doi.org/10.1021/acsami.4c00730
ACS Appl. Mater. Interfaces 2024, 16, 30611−30621

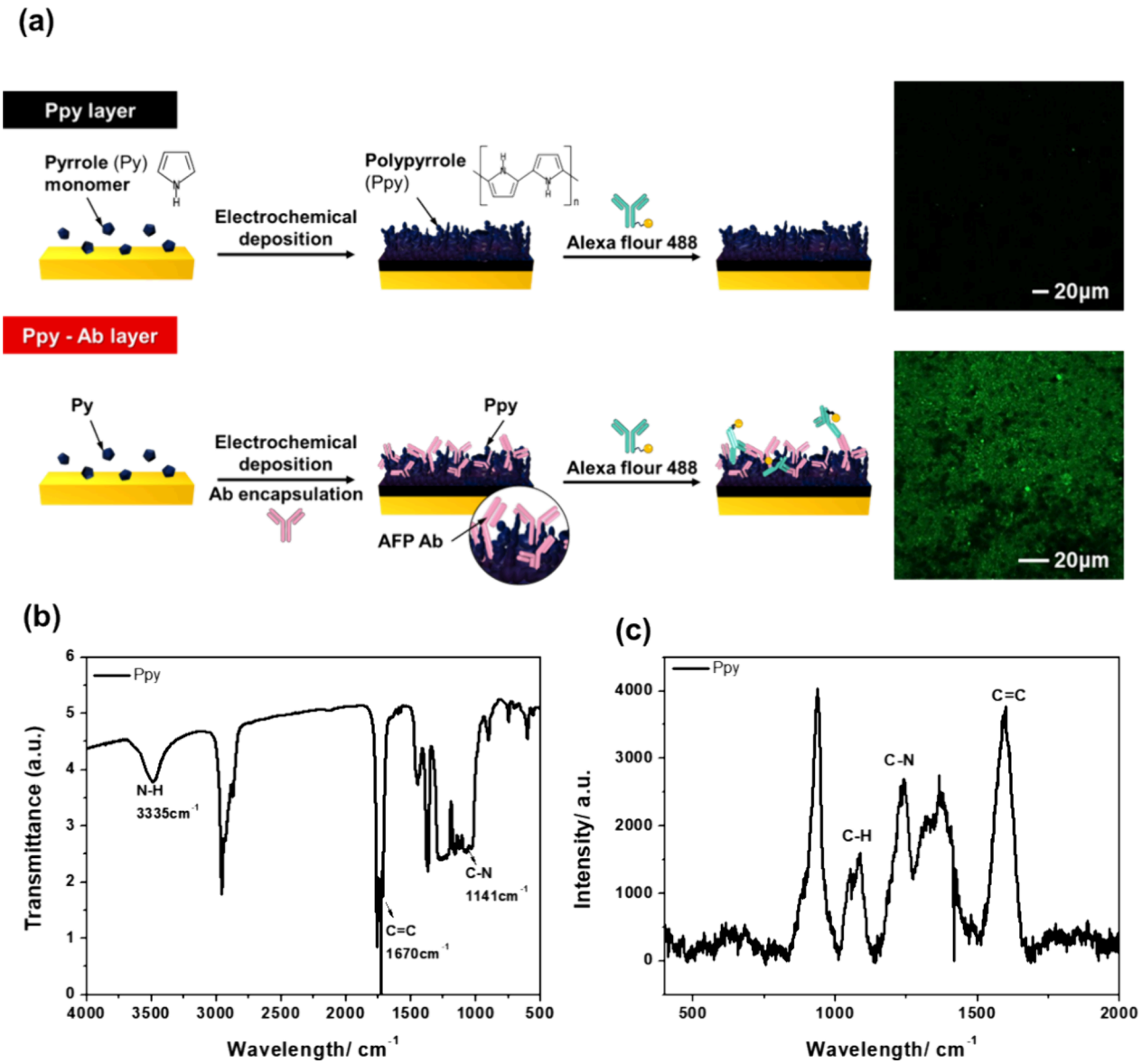

Figure 2. (a) Mechanism of Ppy on the electrode and (b) FTIR and (c) Raman spectroscopy of the Ppy film.

was removed, washed thoroughly with 0.05% PBST three times to remove physically adsorbed Ab and Ag, and prepared for EC measurements.

2.5. Ab Immobilization Using SAMs Based on Covalent Bonding. The electrode was washed with acetone, cleaned with absolute ethanol and DI water, and dried in a stream of N_2. To allow covalent bonding with proteins, the electrodes were first treated with a SAMs. The SPEs were subsequently incubated in 10 mM 11-MUA dissolved in absolute ethanol for 1 h at RT. After washing with absolute ethanol, equal volumes of 400 mM EDC and 100 mM NHS in a pH 4.7 MES buffer were dropped into the SPE and incubated for 10 min to activate the carboxyl groups in the SAMs. Next, a 1 μg/mL anti-AFP Ab was dropped into the SPE and immobilized by covalent bonding between SAMs and Ab in RT for 1 h, followed by FBS (1:10 diluted, for 30 min), which deactivated the non-Ab area in the electrodes, preventing nonspecific binding (Figure 1c). Next, 50 μL of AFP Ag of various concentrations was dropped onto the electrodes and incubated for 30 min at RT. After washing with 0.05% PBST to remove the physically adsorbed Ab and Ag, the electrode was prepared for EC measurements. All washing processes were repeated three times.

2.6. Characterization of the Ppy Modified Electrode. *2.6.1. Confocal Microscopy.* The anti-AFP-modified Ppy composite electrode was prepared as described in Section 2.4. The Ab−Ppy electrode was incubated with 3% BSA. Then, it was immersed in 100 ng/mL goat antimouse IgG (Alexa Fluor 488 labeled) in PBS for 1 h at RT. The Ab−Ppy−SPEs were washed three times with 0.05% PBST, mounted on cover glass using ProLong Gold Antifade Mount (Invitrogen) and visualized using confocal microscopy (LSM 800, ZEISS, Dresden, Germany). Finally, the fluorescence intensity was analyzed using the ImageJ program.

2.6.2. Scanning Electron Microscopy (SEM). SEM micrographs and energy-dispersive X-ray spectroscopy (EDS) images were recorded using a JSM-7610F instrument (JEOL LTD, Japan). Samples were coated with 4 nm thickness before microscopic analyses.

2.6.3. FTIR and Raman Spectroscopy. For Fourier transform infrared (FTIR) characterization, samples were made into KBr disks, and spectra were recorded using a PerkinElmer 2000 spectrometer. Raman spectra were obtained by using a Renishaw 2000 Raman spectrometer.

2.6.4. Electrochemical Characterization. In this study, CV, SWV, and EIS were performed to characterize the EC performance. SPEs were connected to a multichannel potentiostat that measured the EC signal. The SPEs were immersed in an electrolytic conducting solution of 5 mM $[Fe(CN)_6]^{3-/4-}$ + 0.1 M KCl in pH 7.4 PBS at RT.

https://doi.org/10.1021/acsami.4c00730
ACS Appl. Mater. Interfaces 2024, 16, 30611−30621

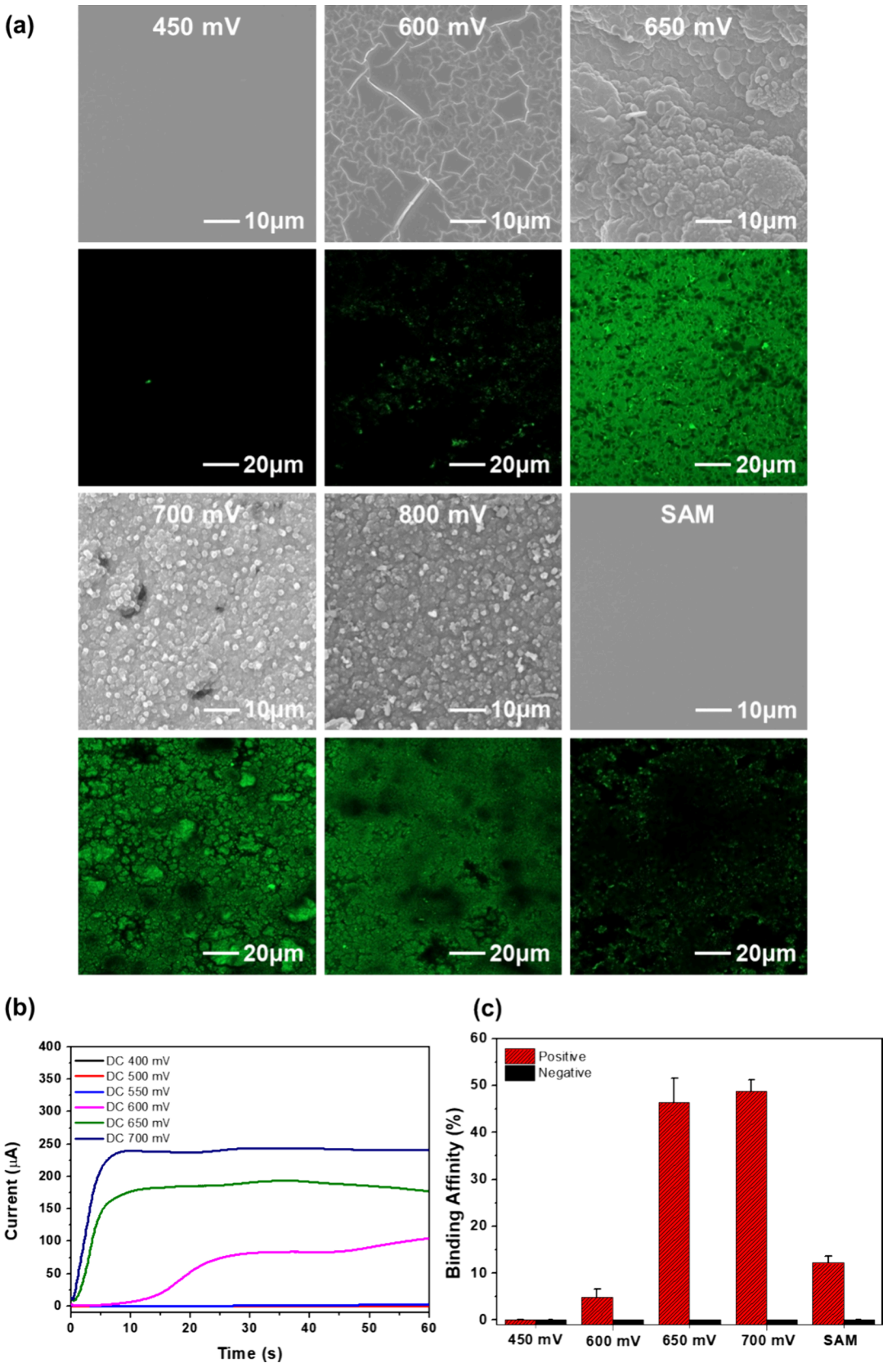

Figure 3. (a) Confocal fluorescence images of the electrode with the Ab−Ppy composite film by DceP with changing potential and the electrode with SEM. Goat antimouse IgG (with Alexa Fluor 488) was labeled. (b) Amperometry curve at 400, 500, 550, 600, 650, 700, and 800 mV in an Ab−pyrrole mixing solution. (c) Comparison of IgG binding affinity based on fluorescence images of the Ab−Ppy composite film (positive) and the only Ppy composite film (negative).

https://doi.org/10.1021/acsami.4c00730
ACS Appl. Mater. Interfaces 2024, 16, 30611−30621

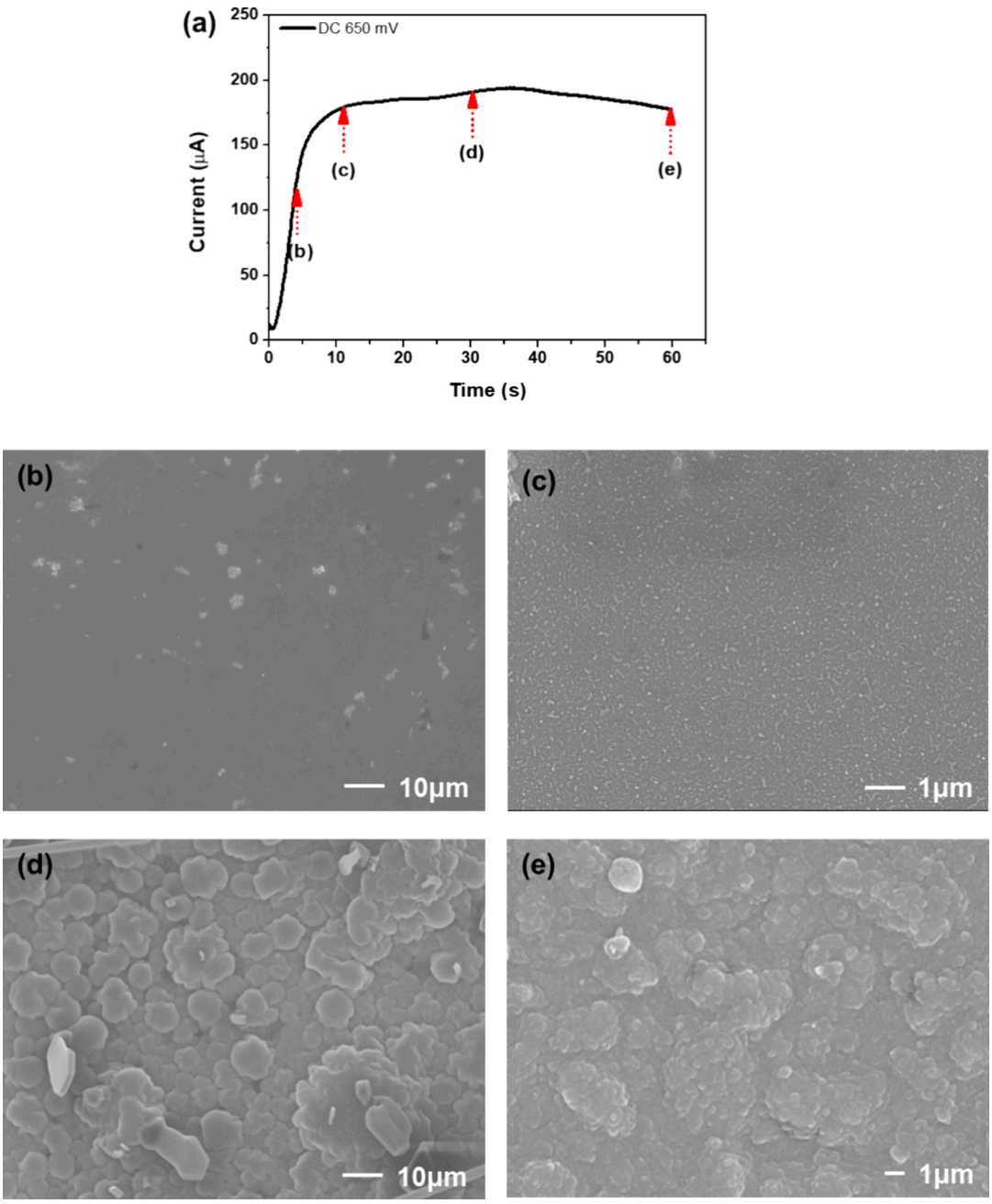

Figure 4. (a) Amperometry curve of DCeP with different polymerization times. SEM images of Ppy morphology according to DCeP time at (b) 5, (c) 10, (d) 30, and (e) 60 s in Ab−pyrrole mixing solutions.

CV was performed at 0.05 V/s, and the potential range was −0.3 to 0.5 V. SWV signals were recorded at each step between −0.3 and 0.5 V, with a step potential (ΔE) of 4 mV, an amplitude (E_{sw}) of 4 mV, and a frequency of 15 Hz. AFP quantification was performed by nonfaradaic EC impedance in PBS as the electrolyte. EIS data were recorded from 1 MHz to 0.5 Hz with a fixed DC potential at the open circuit. All EIS tests were performed at RT, and the data were collected at 10 Hz.

2.6.5. Methods in Statistics. All assays were performed five times, and the mean and standard deviations (SDs) were calculated at each concentration to generate the calibration curve. Each replicate was measured by using a new electrode. The electrolyte was prepared at each measurement time to maintain the fresh conditions. All graphs were created by using the Origin 8.0 program.

3. RESULTS AND DISCUSSION

3.1. Methodology and Characterization of Ab−Ppy Composite Layer. Electropolymerization of pyrrole is accomplished by oxidation of the neutral monomer to a radical cation followed by aromatization and oxidation of the dimer.[36,37] Ppy polymerization proceeds when the potential is sufficiently high to oxidize the monomer. In this work, DCeP based on potentiostatics was performed and the Ab−Ppy layer was generated by electropolymerization of pyrrole. Pyrrole and Ab are distributed in the solution. Once an oxidative potential is applied to the electrode, the Ab and pyrrole monomer near by the electrode make an Ab−Ppy encapsulated layer with growing polymer. As shown in the confocal fluorescence image, any fluorescence intensity could not be observed in the

https://doi.org/10.1021/acsami.4c00730
ACS Appl. Mater. Interfaces 2024, 16, 30611−30621

case of the Ppy layer without adding anti-AFP Ab (only pyrrole in the solution); however, fluorescence intensity could be observed widely in the case of a Ppy layer with added anti-AFP Ab (in Ppy + Ab mixing solution) (Figure 2a). These results demonstrate that the Ab−Ppy recognition layer could be generated by using electropolymerization of pyrrole as a driving force. As shown the Figure 2b,c, the chemical compositions of Ppy electrodes were characterized by FTIR and Raman spectroscopy. The FTIR spectrum of Ppy showed a strong peak near 1670 cm^{-1} due to pyrrole ring stretching,[38] a broad band located at 3333 cm^{-1} is due to N−H stretching vibration, and the band at 1141 cm⁻1 is due to C−N stretching.[39] Raman spectroscopy results show clearly the presence of Ppy and the Raman peaks appear at 1040 cm^{-1} (C−H), 1230 cm^{-1} (C−N), and 1750 cm^{-1} (C═N bonding),[40] respectively. These results confirmed the fabrication of Ppy on the electrodes. The microscopic morphology of the Ab−Ppy composite film on the electrode was characterized by SEM and confocal microscopy. The Ppy structures were polymerized with a DC potential in Ab−pyrrole mixing solutions. As shown in Figure 3a, the SEM morphology of the Ppy composite film changed with the DCeP potential. Ppy was not polymerized at low potential (450 mV), and a micrometer-sized boundary was generated at a potential of 600 mV. The large-cloud morphology was generated at 650 mV, and the small swelling and aggregated morphology were observed below the 700 mV potential. The current−time amperometric curve shows the Ppy polymerization reaction, and the current value increases with increasing DCeP potential (Figure 3b). This means that the electrical conductivity changed with the conditions; therefore, we assume that the Ppy density and thickness changed with the DCep potential. Supporting Information Figure S1a shows the thickness of the film. We found that the thickness started to increase at 650 mV potential and dramatically increased continuously. The Ppy deposition weight also increased with increasing potential (Figure S1b). After the Ppy morphology was observed, the efficiency of the Ab activity of the Ab−Ppy composite film was estimated from the performance of the Ab conjugated with a fluorescent dye (Alexa 488). As shown in Figure 3c, the 650 mV condition has a higher intensity and is distributed more homogeneously than the other conditions. In addition, also, we observed that the Ab−Ppy composite film below 650 mV has a condition having a higher value than the covalent bonding of Ab based on SAMs. The microscopy images also mention the Ppy aggregation state when there is a high amplitude of over 650 mV potential. The Ppy cloud and globular morphology were not observed at 700 mV and 800 mV potentials, and a small Ppy cloud was overlain on the Ppy cloud that was generated previously. We also observed that Au was damaged in some areas because a high potential was continuously applied to the electrode. This reaction was observed under potential conditions of >800 mV (Figure S2). This Ppy aggregation affects the ability of the Ab recognition layer to bind Ag.[41−43] The fluorescence images at 700 and 800 mV show the aggregation of Abs, and the largest aggregation structure must cause diminution of the effective Ab area for binding Ag. Therefore, the superior limit was chosen to be 650 mV.

After optimizing the DCeP potential, we evaluated its influence on the Ppy morphology over time. Figure 4a shows the amperometric current−time (I−t) reaction and its SEM morphology at specific times according to Ppy growth. During the initial polymerization at 5 s, the s current value increased dramatically at that stage. Additionally, some Ppy morphologies that have 1−3 μm size start to generate (Figure 4b), and this small size of Ppy morphology was observed in the wide area on the electrode at a reaction time of 10 s (Figure 4c). The current value is a maximum at 30 s. At this stage, a globular Ppy morphology was produced which has a 4−7 μm size (Figure 4d). The large-cloud morphology was produced by increasing the reaction time and reaction to 60 s, as previously reported (Figure 4e).[44−46] The current value is maintained until 90 s, and the Ppy morphology is very similar to 60 s; therefore, we choose the 60 s value as the polymerization time to make the Ab−Ppy composite layer. After potential and time optimization, we observed the fluorescence image by using low film thickness (128 ± 15 nm, 450 mV DCeP), medium thickness (498 ± 37 nm, 650 mV DCeP), and high thickness (1538 ± 158 nm, 900 mV DCeP), and we optimize that the about 500 nm thickness condition which was polymerized by 650 mV so that it has maximum intensity compared with other conditions (Figure S3a). This is correlated with the Ab density result, which was previously shown at Figure 3a. Ab density was increased with DCeP until 700 mV. However, overpotential (above 800 mV) makes the Ppy thicker but damages the electrode (Figure S3b). Table 1 shows the optimized experimental variables.

Table 1. Optimization of the Experimental Variables Affecting the Performance of Ppy−AFP Immunosensor

Variable	Tested	Selected
DC potential (DCep)	550−800 mV	650 mV
Polymerization time	0−60 s	60 s
Ppy thickness	128−1500 nm	near 500 nm

3.2. Nonfaradaic EIS Detection of AFP Using Ppy Immunosensor. In order to fully understand the sensing performance of the Ppy EC immunosensor, we evaluated the EC properties of each electrode. First, CV and SWV measurements were conducted to study the EC behavior of the Ab−Ppy electrode at each stage of modification by changing the DCeP potential. As shown in Figure S4, the EIS curve and impedance increased in the frequency range of 1−10 kHz at 400 and 500 mV DCeP potentials. However, the impedance value starts to decrease at the 550 mV DCeP potential condition, which means that Ppy was generated, which has high conductivity. In this study, the impedance paper and value were recorded in the low-frequency region because the difference was observed at this frequency. We assumed that the EC signal of Ag binding to the Ab−Ppy recognition layer on the electrode is dominated by the interfacial capacitance of the system. Our previous work and other work used EIS immunosensors that are used in the low-frequency region of 4−100 Hz.[47−49] After optimization of the Ppy and recording conditions, EDS spectra were obtained to quantitatively analyze the elemental composition of the fabricated Ppy film and Ab−Ppy composite film (Figure 5a, Table 2). The Au material was quantitatively reduced from 75 to 50% after Ppy polymerization. When an Ab−Ppy film was generated on the number of elements of the electrode, N and O increased compared with those of the other electrode. These changes indicated that the functional group of Ab with −COOH and $-NH_2$ were observed on the electrode.[50] Additionally, Ab was controlled when we prepared the pyrrole

https://doi.org/10.1021/acsami.4c00730
ACS Appl. Mater. Interfaces 2024, 16, 30611−30621

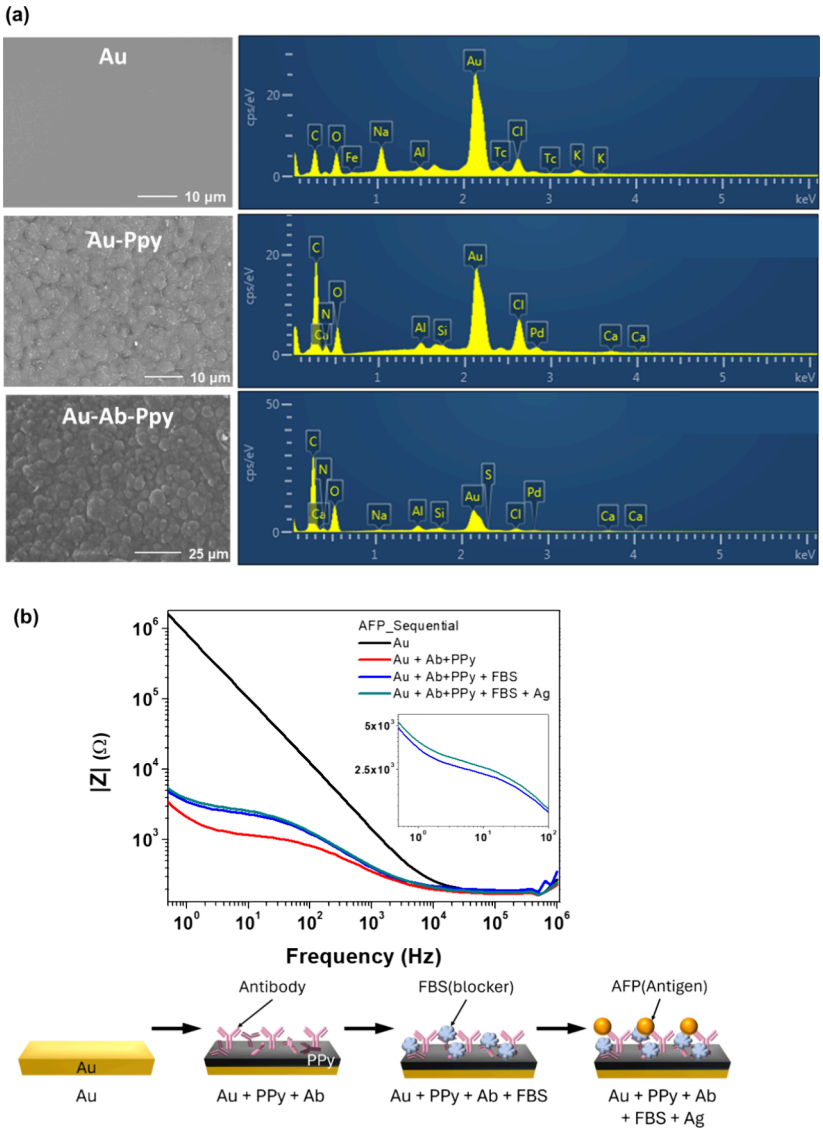

Figure 5. (a) SEM images of the Au, Au−Ppy, and Au−Ab−Ppy composite films and EDS analyses. The atomic fraction of the elements of the film was analyzed by EDS. (b) EIS curves of different modified electrodes.

Table 2. Weight Percent of Each Sample Measured by EDS

	wt %		
	Au	Au−Ppy	Au−Ppy + Ab
Carbon	5.63	23.50	20.96
Au	75.89	49.66	27.53
Oxygen	8.78	14.76	29.97
Nitrogen		5.84	15.91

and Ab mixing solutions. As shown in the confocal image, the Ab concentration in the mixing solution increased and the fluorescence intensity increased (Figure S5). EC results also show Ab immobilization on the electrodes. As shown the Figure S6, the faradaic region (redox region) and nonfaradaic region (charge/discharge region) were decreased with increasing Ab concentrations. It means more anti-AFP Ab was bound to the electrode, making a denser, thicker insulation layer to be generated on the electrode. Considering these results, we know that (1) Ab was encapsulated in the Ppy layer and (2) a high-density Ab layer could be generated by adding high concentrations of Ab in the Ppy mixing solutions. In order to fully understand immobilization, a nonfaradaic EIS test was performed. Compared with the Au baseline, the impedance value dramatically decreased after the immobilization of Ab−Ppy because Ppy facilitates the electron transfer speed of the sensing interface.[51] Next, we dropped the 1:10 FBS solution to block nonspecific binding, and the nonspecific and impedance increased due to the low electric permittivity of the FBS. After AFP, specific Ag was incubated on the electrode, and the impedance was further increased because of the low conductivity of AFP. The change in impedance recorded after being combined with AFP confirmed the feasibility of the immunosensor (Figure 5b). The sensing performance of the Ab−Ppy immunosensor was characterized by performing nonfaradaic EIS tests in 10 mM PBS after immobilization with various AFP concentrations.

In this work, impedance change was calculated to quantify AFP, and it was determined by following eq 1.

https://doi.org/10.1021/acsami.4c00730
ACS Appl. Mater. Interfaces 2024, 16, 30611−30621

quantification of AFP by magnitude of impedance:

$$\text{impedance change}/\% = \frac{|Z|}{|Z|_0} = \frac{|Z|_{Ab-Ag} - |Z|_{FBS}}{|Z|_{FBS}} \quad (1)$$

where $|Z|_{Ab-Ag}$ is the impedance value at 10 Hz as AFP binds to the AFP antibody on the Ppy immunosensor. $|Z|_{FBS}$ is the value after blocking FBS for nonspecific binding as a baseline. Panels a and b of Figure 6 show the relationship between the change

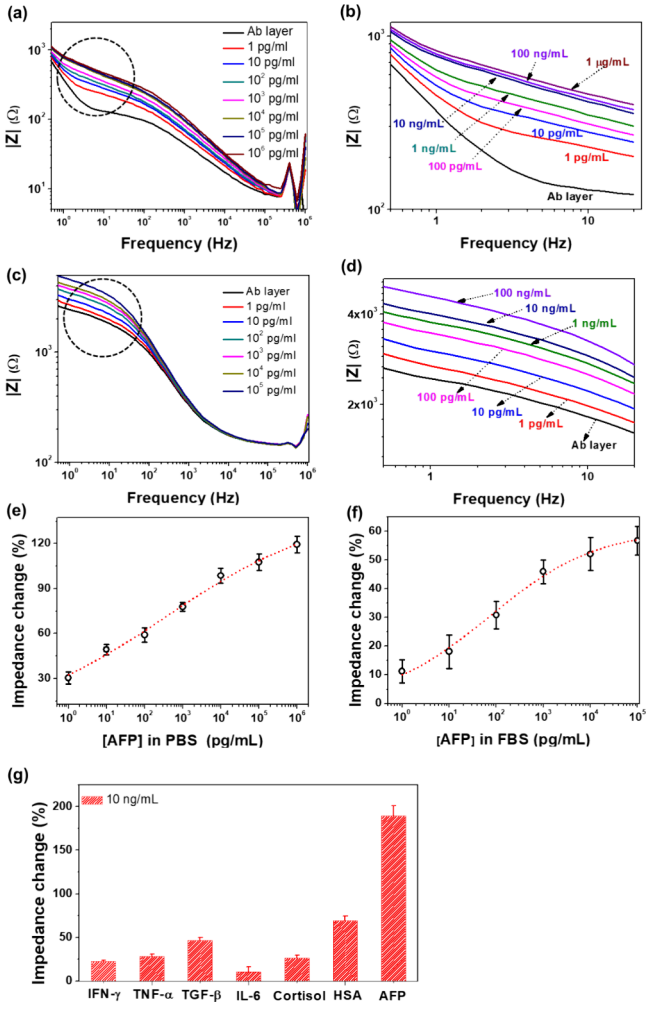

Figure 6. EIS curves at various concentrations of AFP via EC measurement in PBS using (a) an electrode with an AFP Ab−Ppy composite layer and (b) expansion of the frequency region from 0.1 to 20 Hz as designated on panel a. EIS with curves at various concentrations of AFP in FBS using the (c) electrode an AFP Ab−Ppy composite layer and (d) expansion of the frequency region from 0.1 to 20 Hz as desinated on panel c. The EIS curves were measured by using PBS as an electrolyte. Calibration curves of the AFP in (e) PBS and (f) FBS. (g) Selectivity test of the electrode with the AFP Ab−Ppy layer (n = 5).

in the impedance signal at 10 Hz, for which the signal is dominated by the dielectric behavior of the electrode surface, and the logarithm of the concentration of AFP, with the concentration ranging from 1 pg/mL to 1 μg/mL. In the signal for the negative control (without Ab) Ppy immunosensor, the impedance was not significantly changed because AFP did not bind to the Ppy immunosensor (Figure S7a). AFP was also calibrated in 10% FBS (in which there are other proteins and cells but insignificant amounts of AFP). In these conditions, impedance increased with increasing AFP concentrations, and it shows a result similar to that from the AFP measurement in PBS (Figure 6c,d). Additionally, the signal for negative control (without Ab) detection in FBS was not changed compared to the positive control (Figure S7b). The AFP calibration plot is shown in Figure 6e,f. The LODs of AFP were estimated to be 3.13 (PBS) and 43.86 (FBS), respectively. In this calibration plot, the LOD was estimated by gathering the impedance signal of the zero-concentration value plus three times its SD.[52] The selectivity test was performed for the specific detection of the AFP Ppy immunosensor to target AFP by choosing some interference proteins such as interferon-γ (IFN-γ), IL-6, cortisol, human serum albumin, tumor necrosis factor-α (TNF-α), and transforming growth factor-β (TGF-β). As shown in Figure 6g, this Ppy immunosensor only showed a significant impedance change to AFP compared with other interfering proteins. This indicates that the Ppy immunosensor can detect AFP. Finally, repeatability and reproducibility tests were performed by measuring by using various concentrations of AFP (low, 10 pg/mL; medium, 1 ng/mL; high, 100 ng/mL) under the same status (Figur S8) and the RSDs (relative standard deviations) are 6.67, 6.42, and 7.54%, respectively. The reproducibility test was also performed. The reproducibility of the AFP biosensor was measured by using the developed electrode constructed under the same test conditions. The impedance signal was measured by using various concentrations of AFP (low, 10 pg/mL; medium, 1 ng/mL; high, 100 ng/mL) and the RSDs are 7.58, 7.67, and 10.70%., respectively. Figure S9a showed the results of the stability of the Ppy immunosensor and the EIS curves of fresh conditions and after 5 days were compared, and we found that their EIS curves perfectly overlapped. Figure S9b shows the degradation durability result and the impedance signal before and after AFP binding using a set of Ppy immunosensors for 10 days, showing excellent stability. Considering the results obtained for the Ppy immunosensor, we compared it to the other AFP biosensors mentioned in Table 3. Our AFP immunosensor based on DCeP of the Ab−Ppy composite film exhibited (1) excellent Ab immobilization time, which we called "rapid coating", and (2) high sensitivity and selectivity. Although the Ab orientation problem still should be solved, we performed to achieve Ab orientation by additional coating protein G or AuNp or magnetic particle. These results in this work are considerable because the rapid and direct coating of the Ab layer was consistent in 1 min. It is a quick and simple step and easy, so anyone can use this method anywhere. In addition, material, whether a polar or nonpolar group and regardless of its size from nm to μm, could be coated on the electrode by a rapid coating method. Based on this, we are developing a platform that can be applied to an infectious disease that can be applied to on-site diagnosis.

4. CONCLUSIONS

In this study, we presented the development of an AFP quantification of EC biosensor composed of an Ab−Ppy composite layer. DCeP was performed to polymerize pyrrole, and during polymerization, Ab was also coated on the Ppy layer. We optimized Ab density by controlling the polymerization time and potential. Finally, 74% of Ab with high density was coated on the electrode in 1 min. This process is fast compared with conventional SAMs, and direct coating is possible without any additional supporting material such as a

https://doi.org/10.1021/acsami.4c00730
ACS Appl. Mater. Interfaces 2024, 16, 30611−30621

Table 3. Comparison of the AFP Immunosensors[a]

Method	Material	Range	LOD	Sample prep time	Ref
Giant magnetoimpedance	$Co_{68.2}Fe_{4.3}Si_{12.5}B_{15}$ glass-coated amorphous wire/MB-labeled AFP antibody	100 fg/mL to 1 μg/mL	1 fg/mL	1 day (24 h)	53
Microcantilever array sensing	Gold-coated rectangular microcantilever/aptamer	1−900 ng/mL	0.6 ng/mL	1 h	54
Microcantilever array sensing	SiO_2 microcavity of the cantilever/AuNPs functionalized detection antibody	0−70 ng/mL	21 pg/mL	12 h (4°)	55
Photoelectrochemical assay	TiO_2 and the conjugated polymer/antibody	100 pg/mL to 100 ng/mL	30 pg/mL	Overnight (12 h)	56
EC assay	Polyaniline/BSA/silver nanoparticle immobilization matrix/antibody	10 pg/mL to 10 ng/mL	4.7 pg/mL	48 h (4°)	57
EC assay	Thi and AuNPs comodified with rGO-TEPA-Au)/ antibody	5 pg/mL to 100 ng/mL	2.2 pg/mL	2 h (RT)	58
EC assay	PtNps/rGO−COOH-modified SPGE/Aptamer	3−30 ng/mL	1.22 ng/mL	45 min (RT)	59
EC assay	Ab-Ppy composite layer	1 pg/mL to 100 ng/mL	3.13 pg/mL (PBS); 43.86 pg/mL (FBS)	1 min (RT)	This work

[a]MB, magnetic beads; Thi, thionine; AuNPs, gold nanoparticles; rGO, reduced graphene oxide; Thi, thionine; SPGE, screen-printed graphene carbon paste electrode; PtNPs, platinum nanoparticles; TEPA, tetraethylenepentamine.

nanoparticle. Moreover, a high and rigid Ab recognition layer was consistent on the electrode. Next, AFPs in the PBS and serum were quantified, and the LODs of AFP were estimated to be 3.13 pg/mL (PBS) and 43.86 pg/mL (FBS), respectively. This AFP sensor exhibits satisfying sensitivity, selectivity, reproducibility, and stability. This AFP EC sensors can become a valuable tool for point-of-care biomarker assessment.

■ ASSOCIATED CONTENT

Supporting Information

The Supporting Information is available free of charge at https://pubs.acs.org/doi/10.1021/acsami.4c00730.

Ppy thickness and weight; additional SEM images; EIS curves of different synthetic conditions; confocal images of Ab-Ppy composite film; EIS curves by using an electrode with only Ppy composite layer; reproducibility and repeatability; stability results (PDF)

■ AUTHOR INFORMATION

Corresponding Author

JuKyung Lee − *Digital Healthcare Research Center, Gumi Electronics and Information Technology Research Institute (GERI), Gumi, Gyeongbuk 39253, Republic of Korea;* orcid.org/0000-0002-2751-8112; Email: chejueyes@geri.re.kr

Authors

USun Nam − *Department of Medical IT Convergence, Kumoh National Institute of Technology, Gumi, Gyeongbuk 39177, Republic of Korea;* orcid.org/0009-0006-0280-301X

Han Na Suh − *Korea Institute of Toxicology (KIT), Jeongeup, Jeollabuk-do 56212, Republic of Korea;* orcid.org/0000-0002-7647-7249

Sang-Keun Sung − *Digital Healthcare Research Center, Gumi Electronics and Information Technology Research Institute (GERI), Gumi, Gyeongbuk 39253, Republic of Korea*

ChaeWon Seo − *Department of Medical IT Convergence, Kumoh National Institute of Technology, Gumi, Gyeongbuk 39177, Republic of Korea*

Jung Hyun Lee − *Department of Dermatology, School of Medicine and Institute for Stem Cell and Regenerative Medicine, University of Washington, Seattle, Washington 98109, United States*

Jeong Yoon Lee − *The Laboratory of Viromics and Evolution, Korea Zoonosis Research Institute, Jeonbuk National University, Iksan-si, Jeollabuk-do 54531, Republic of Korea*

SangHee Kim − *Department of Medical IT Convergence, Kumoh National Institute of Technology, Gumi, Gyeongbuk 39177, Republic of Korea*

Complete contact information is available at: https://pubs.acs.org/10.1021/acsami.4c00730

Author Contributions

US.N.: methodology, investigation, and data validation. H.N.S.: data curation and resources. S.-K.S.: data curation and investigation. C.W.S.: investigation. J.H.L.: investigation. J.Y.L.: data curation and resources. S.H.K.: resources and supervision. J.K.L.: conceptualization and supervision. US.N. and H.N.S. contributed equally as first authors.

Notes

The authors declare no competing financial interest.

■ ACKNOWLEDGMENTS

This work was supported by the project for Industry-University-Research Institute platform cooperation R&D funded by Korea Ministry of SMEs and Startups in 2022 (S3310771) and "Regional Innovation Strategy (RIS)" through the National Research Foundation of Korea (NRF) funded by the Ministry Education (MOE) (2022RIS-006) and the Elsa U Pardee Foundation, MCC patient gift fund.

■ REFERENCES

(1) Felix, F. S.; Angnes, L. Electrochemical Immunosensors−A Powerful Tool for Analytical Applications. *Biosens. Bioelectron.* **2018**, *102*, 470−478.

(2) Burcu Bahadır, E.; Kemal Sezginturk, M. Applications of Electrochemical Immunosensors for Early Clinical Diagnostics. *Talanta* **2015**, *132*, 162−174.

(3) Verma, N.; Bhardwaj, A. Biosensor Technology for Pesticides—A Review. *Biotechnol. Appl. Biochem.* **2015**, *175*, 3093−3119.

(4) Belkhamssa, N.; Justino, C. I.; Santos, P. S.; Cardoso, S.; Lopes, I.; Duarte, A. C.; Rocha-Santos, T.; Ksibi, M. Label-Free Disposable Immunosensor for Detection of Atrazine. *Talanta* **2016**, *146*, 430−434.

(5) Aydin, S. A Short History, Principles, and Types of ELISA, and Our Laboratory Experience with Peptide/Protein Analyses Using ELISA. *Peptides* **2015**, *72*, 4−15.

(6) Chen, C.; Zhao, J.; Lu, Y.; Sun, J.; Yang, X. Fluorescence Immunoassay Based on The Phosphate-Triggered Fluorescence Turn-on Detection of Alkaline Phosphatase. *Anal. Chem.* **2018**, *90*, 3505−3511.
(7) Luz, J. G.; Souto, D. E.; Machado-Assis, G. F.; de Lana, M.; Kubota, L. T.; Luz, R. C.; Damos, F.; Martins, H. Development and Evaluation of A SPR-Based Immunosensor for Detection of Anti-Trypanosoma Cruzi Antibodies in Human Serum. *Sens. Actuators, B* **2015**, *212*, 287−296.
(8) Marques, R. C.; Costa-Rama, E.; Viswanathan, S.; Nouws, H. P.; Costa-Garcia, A.; Delerue-Matos, C.; González-García, M. B. Voltammetric Immunosensor for The Simultaneous Analysis of the Breast Cancer Biomarkers CA 15−3 and HER2-ECD. *Sens. Actuators, B* **2018**, *255*, 918−925.
(9) Talib, N. A. A.; Salam, F.; Sulaiman, Y. Development of Highly Sensitive Immunosensor for Clenbuterol Detection by Using Poly (3, 4-Ethylenedioxythiophene)/Graphene Oxide Modified Screen-Printed Carbon Electrode. *Sensors* **2018**, *18*, 4324.
(10) Singh, A. C.; Bacher, G.; Bhand, S. A Label Free Immunosensor for Ultrasensitive Detection of 17β-Estradiol in Water. *Electrochim. Acta* **2017**, *232*, 30−37.
(11) Monerris, M. J.; Arévalo, F. J.; Fernández, H.; Zon, M. A.; Molina, P. G. Development of A Very Sensitive Electrochemical Immunosensor for The Determination of 17β-Estradiol in Bovine Serum Samples. *Sens. Actuators, B* **2015**, *208*, 525−531.
(12) Windmiller, J. R.; Wang, J. Wearable Electrochemical Sensors and Biosensors: A Review. *Electroanalysis* **2013**, *25*, 29−46.
(13) Tong, X.; Ga, L.; Bi, L.-G.; Ai, J. Wearable Electrochemical Sensors Based on Nanomaterials for Healthcare Applications. *Electroanalysis* **2023**, *35*, No. e202200228.
(14) Lee, J.-K.; Noh, G.-H.; Pyun, J.-C. Capacitive Immunoaffinity Biosensor by Using Diamond-Like Carbon (DLC) Electrode. *Biochip J.* **2009**, *3* (4), 287−292.
(15) Lee, J.; Bubar, C. T.; Moon, H. G.; Kim, J.; Busnaina, A.; Lee, H.; Shefelbine, S. J. Measuring Bone Biomarker Alkaline Phosphatase with Wafer-Scale Nanowell Array Electrodes. *ACS Sens.* **2018**, *3*, 2709−2715.
(16) Zhang, L.; Mazouzi, Y.; Salmain, M.; Liedberg, B.; Boujday, S. Antibody-Gold Nanoparticle Bioconjugates for Biosensors: Synthesis, Characterization and Selected Applications. *Biosens. Bioelectron.* **2020**, *165*, No. 112370.
(17) Shen, M.; Rusling, J. F.; Dixit, C. K. Site-Selective Orientated Immobilization of Antibodies and Conjugates for Immunodiagnostics Development. *Methods* **2017**, *116*, 95−111.
(18) Welch, N. G.; Scoble, J. A.; Muir, B. W.; Pigram, P. J. Orientation and Characterization of Immobilized Antibodies for Improved Immunoassays. *Biointerphases* **2017**, *12* (2), No. 02D301.
(19) Gajos, K.; Szafraniec, K.; Petrou, P.; Budkowski, A. Surface Density Dependent Orientation and Immunological Recognition of Antibody on Silicon: TOF-SIMS and Surface Analysis of Two Covalent Immobilization Methods. *Appl. Surf. Sci.* **2020**, *518*, No. 146269.
(20) Ramanaviciene, A.; Ramanavicius, A. Application of Polypyrrole for The Creation of Immunosensors. *Crit. Rev. Anal. Chem.* **2002**, *32*, 245−252.
(21) Jia, Q.; Ma, X.; Chen, H.; Li, X.; Huang, M.-H. Unusual 3, 4-Oxidative Coupling Polymerization on 1, 2, 5-Trisubstituted Pyrroles for Novel Porous Organic Polymers. *ACS Macro Lett.* **2023**, *12*, 1358−1364.
(22) Atta, A.; Negm, H.; Abdeltwab, E.; Rabia, M.; Abdelhamied, M. M. Facile Fabrication of Polypyrrole/NiOx Core-Shell Nanocomposites for Hydrogen Production from Wastewater. *Polym. Adv. Technol.* **2023**, *34*, 1633−1641.
(23) Gao, M.; Dai, L.; Wallace, G. G. Glucose Sensors Based on Glucose-Oxidase-Containing Polypyrrole/Aligned Carbon Nanotube Coaxial Nanowire Electrodes. *Synth. Met.* **2003**, *137*, 1393−1394.
(24) Tamiya, E.; Karube, I.; Hattori, S.; Suzuki, M.; Yokoyama, K. Micro Glucose Using Electron Mediators Immobilized on A Polypyrrole-Modified Electrode. *Sens. Actuators* **1989**, *18*, 297−307.
(25) Cesarino, I.; Galesco, H. V.; Moraes, F. C.; Lanza, M. R.; Machado, S. A. Biosensor Based on Electrocodeposition of Carbon Nanotubes/Polypyrrole/Laccase for Neurotransmitter Detection. *Electroanalysis* **2013**, *25*, 394−400.
(26) Ramya, R.; Sangaranarayanan, M. V. Polypyrrole Microfibres Synthesized with Quillaja Saponin for Sensing of Catechol. *Sens. Actuators, B* **2012**, *173*, 40−51.
(27) Pennetta, C.; Floresta, G.; Graziano, A. C. E.; Cardile, V.; Rubino, L.; Galimberti, M.; Rescifina, A.; Barbera, V. Functionalization of Single and Multi-Walled Carbon Nanotubes with Polypropylene Glycol Decorated Pyrrole for The Development of Doxorubicin Nano-Conveyors for Cancer Drug Delivery. *Nanomaterials* **2020**, *10*, 1073.
(28) Shah, S. A. A.; Firlak, M.; Berrow, S. R.; Halcovitch, N. R.; Baldock, S. J.; Yousafzai, B. M.; Hathout, R. M.; Hardy, J. G. Electrochemically Enhanced Drug Delivery Using Polypyrrole Films. *Materials.* **2018**, *11*, 1123.
(29) Galle, P. R.; Foerster, F.; Kudo, M.; Chan, S. L.; Llovet, J. M.; Qin, S.; Schelman, W. R.; Chintharlapalli, S.; Abada, P. B.; Sherman, M.; Zhu, A. X. Biology and Significance of Alpha-Fetoprotein in Hepatocellular Carcinoma. *Liver Int.* **2019**, *39*, 2214−2229.
(30) Nouso, K.; Kobayashi, Y.; Nakamura, S.; Kobayashi, S.; Takayama, H.; Toshimori, J.; Kuwaki, K.; Hagihara, H.; Onishi, H.; Miyake, Y.; Ikeda, F.; Shiraha, H.; Takaki, A.; Iwasaki, Y.; Kobashi, H.; Yamamoto, K. Prognostic Importance of Fucosylated Alpha-Fetoprotein in Hepatocellular Carcinoma Patients with Low Alpha-Fetoprotein. *J. Gastroenterol. Hepatol.* **2011**, *26*, 1195−1200.
(31) Burditt, L. J.; Johnson, M. M.; Johnson, P. J.; Williams, R. Detection of Hepatocellular Carcinoma-Specific Alpha-Fetoprotein by Isoelectric Focusing. *Cancer* **1994**, *74*, 25−29.
(32) Hu, X.; Chen, R.; Wei, Q.; Xu, X. The Landscape of Alpha Fetoprotein in Hepatocellular Carcinoma: Where Are We? *Int. J. Biol. Sci.* **2022**, *18*, 536−551.
(33) Zheng, Y.; Zhu, M.; Li, M. Effects of Alpha-Fetoprotein on the Occurrence and Progression of Hepatocellular Carcinoma. *J. Cancer Res. Clin. Oncol.* **2020**, *146*, 2439−2446.
(34) Aydın, E. B.; Aydın, M.; Sezgintürk, M. K. Fabrication of Electrochemical Immunosensor based on Acid-Substituted Poly (pyrrole) Polymer Modified Disposable ITO Electrode for Sensitive Detection of CCR4 Cancer Biomarker in Human Serum. *Talanta* **2021**, *222*, No. 121487.
(35) Gu, Y.; Wang, J.; Pan, M.; Li, S.; Fang, G.; Wang, S. Label-Free Impedimetric Immunosensor Based on One-Step Co-Electrodeposited Poly-(pyrrole-co-pyrrole-1-propionic acid) and Reduced Graphene Oxide Polymer Modified Layer for The Determination of Melamine. *Sens. Actuators, B* **2019**, *283*, 571−578.
(36) Ansari, R. Polypyrrole Conducting Electroactive Polymers: Synthesis and Stability Studies. *J. Chem.* **2006**, *3*, 860413.
(37) Dubal, D. P.; Patil, S. V.; Kim, W. B.; Lokhande, C. D. Supercapacitors Based on Electrochemically Deposited Polypyrrole Nanobricks. *Mater. Lett.* **2011**, *65*, 2628−2631.
(38) Singu, B. S.; Yoon, K. R. Mesoporous Polypyrrole-Ag Nanocomposites for Supercapacitors. *J. Alloy. Comp.* **2018**, *742*, 610−618.
(39) Hussain, S. K.; Dudem, B.; Yu, J. S. Enhanced Electrochemical Performance via PPy Encapsulated 3D Flower-like Bismuth Molybdate Nanoplates for High-performance Supercapacitors. *Appl. Surf. Sci.* **2019**, *478*, 846−856.
(40) Arteaga, G. C.; Del Valle, M. A.; Antilén, M.; Romero, M.; Ramos, A.; Hernández, L.; Arévalo, M. C.; Pastor, E.; Louarn, G. Nucleation and Growth Mechanism of Electro-synthesized Poly (pyrrole) on Steel. *Int. J. Electrochem. Sci.* **2013**, *8*, 4120−4130.
(41) Gonçalves, M. D. L.; Truta, L. A.; Sales, M. G. F.; Moreira, F. T. Electrochemical Point-of Care (PoC) Determination of Interleukin-6 (IL-6) Using A Pyrrole (Py) Molecularly Imprinted Polymer (MIP) on A Carbon-Screen Printed Electrode (C-SPE). *Anal. Lett.* **2021**, *54*, 2611−2623.

https://doi.org/10.1021/acsami.4c00730
ACS Appl. Mater. Interfaces 2024, 16, 30611−30621

(42) C. G., A. M.; Varghese, A.; M., N. Recent Advances in Nanomaterials Based Molecularly Imprinted Electrochemical Sensors. *Crit. Rev. Anal. Chem.* **2023**, *53*, 88−97.
(43) Awokoya, K. N.; Okoya, A. A.; Elujulo, O. Preparation, Characterization and Evaluation of A Styrene-Based Molecularly Imprinted Polymer for Capturing Pyridine and Pyrrole From Crude Oil. *Sci. Afr.* **2021**, *13*, No. e00947.
(44) Wencheng, S.; Iroh, J. O. Effects of Electrochemical Process Parameters on The Synthesis and Properties of Polypyrrole Coatings on Steel. *Synth. Met.* **1998**, *95*, 159−167.
(45) Fabregat-Santiago, F.; Mora-Seró, I.; Garcia-Belmonte, G.; Bisquert, J. Cyclic Voltammetry Studies of Nanoporous Semiconductors. Capacitive and Reactive Properties of Nanocrystalline TiO2 Electrodes in Aqueous Electrolyte. *J. Phys. Chem. B* **2003**, *107*, 758−768.
(46) Lee, J.; Jeong, H.; Lassarote Lavall, R.; Busnaina, A.; Kim, Y.; Jung, Y. J.; Lee, H. Polypyrrole Films with Micro/Nanosphere Shapes for Electrodes of High-Performance Supercapacitors. *ACS Appl. Mater. Interfaces* **2017**, *9*, 33203−33211.
(47) Lee, J.; Bubar, C. T.; Moon, H. G.; Kim, J.; Busnaina, A.; Lee, H.; Shefelbine, S. J. Measuring Bone Biomarker Alkaline Phosphatase with Wafer-Scale Nanowell Array Electrodes. *ACS Sens.* **2018**, *3*, 2709−2715.
(48) Lee, J.; Shin, S.; Desalvo, A.; Lee, G.; Lee, J. Y.; Polini, A.; Chae, S.; Jeong, H.; Kim, J.; Choi, H.; Lee, H. Nonmediated, Label-Free Based Detection of Cardiovascular Biomarker in a Biological Sample. *Adv. Healthcare Mater.* **2017**, *6*, No. 1700231.
(49) Patil, A. V.; Bedatty Fernandes, F. C.; Bueno, P. R.; Davis, J. J. Immittance Electroanalysis in Diagnostics. *Anal. Chem.* **2015**, *87*, 944−950.
(50) Lorenzen, A. L.; Dos Santos, A. M.; Dos Santos, L. P.; da Silva Pinto, L.; Conceição, F. R.; Wolfart, F. PEDOT-AuNPs-based Impedimetric Immunosensor for The Detection of SARS-CoV-2 Antibodies. *Electrochim. Acta* **2022**, *404*, No. 139757.
(51) Song, J.; Teng, H.; Xu, Z.; Liu, N.; Xu, L.; Liu, L.; Gao, F.; Luo, X. Free-Standing Electrochemical Biosensor for Carcinoembryonic Antigen Detection Based on Highly Stable and Flexible Conducting Polypyrrole Nanocomposite. *Microchim. Acta* **2021**, *188*, 217.
(52) Lauria, I.; Kramer, M.; Schröder, T.; Kant, S.; Hausmann, A.; Böke, F.; Leube, R.; Telle, R.; Fischer, H. Inkjet Printed Periodical Micropatterns Made of Inert Alumina Ceramics Induce Contact Guidance and Stimulate Osteogenic Differentiation of Mesenchymal Stromal Cells. *Acta Biomater.* **2016**, *44*, 85−96.
(53) Zhu, Y.; Zhang, Q.; Li, X.; Pan, H.; Wang, J.; Zhao, Z. Detection of AFP with An Ultra-Sensitive Giant Magnetoimpedance Biosensor. *Sens. Actuators, B* **2019**, *293*, 53−58.
(54) Li, C.; Ma, X.; Guan, Y.; Tang, J.; Zhang, B. Microcantilever Array Biosensor for Simultaneous Detection of Carcinoembryonic Antigens and α-Fetoprotein Based on Real-Time Monitoring of The Profile of Cantilever. *ACS Sens.* **2019**, *4*, 3034−3041.
(55) Zhao, J.; Wang, L.; Fu, D.; Zhao, D.; Wang, Y.; Yuan, Q.; Zhu, Y.; Yang, J.; Yang, F. Gold Nanoparticles Amplified Microcantilever Biosensor for Detecting Protein Biomarkers with High Sensitivity. *Sens. Actuators, A* **2021**, *321*, No. 112563.
(56) Mo, X.; Wang, Y.; Xiao, Q.; Zhou, X.; Li, H. Conjugated Polymer Sensitized Hyperbranched Titanium Dioxide Based Photoelectrochemical Biosensor for Detecting AFP in Serum. *Surf. Interfaces* **2021**, *24*, No. 101103.
(57) Amarnath, C. A.; Sawant, S. N. Polyaniline Based Electrochemical Biosensor for α-Fetoprotein Detection Using Bio-Functionalized Nanoparticles as Detection Probe. *Electroanalysis* **2020**, *32*, 2415−2421.
(58) Xiao, H.; Wei, S.; Gu, M.; Chen, Z.; Cao, L. A Sandwich-Type Electrochemical Immunosensor Using rGO-TEPA-Thi-Au as Sensitive Platform and CMK-3@ AuPtNPs as Signal Probe for AFP Detection. *Microchem. J.* **2021**, *170*, No. 106641.
(59) Upan, J.; Youngvises, N.; Tuantranont, A.; Karuwan, C.; Banet, P.; Aubert, P. H.; Jakmunee, J. A Simple Label-Free Electrochemical Sensor for Sensitive Detection of Alpha-Fetoprotein Based on Specific Aptamer Immobilized Platinum Nanoparticles/Carboxylated-Graphene Oxide. *Sci. Rep.* **2021**, *11*, 13969.

https://doi.org/10.1021/acsami.4c00730
ACS Appl. Mater. Interfaces 2024, 16, 30611−30621